Journal of Molecular Catalysis A: Chemical 297 (2009) 142–149

Contents lists available at ScienceDirect

Journal of Molecular Catalysis A: Chemical

journal homepage: www.elsevier.com/locate/molcata

Selective oxidation of CH_4 and C_2H_6 over a mixed oxygen ion and electron conducting perovskite—A TAP and membrane reactors study

Evgenii V. Kondratenko[a,*], Haihui Wang[b,c], Vita A. Kondratenko[a], Jürgen Caro[b]

[a] Leibniz-Institut für Katalyse e. V. an der Universität Rostock, Aussenstelle Berlin, Richard-Willstätter-Str. 12, D-12489 Berlin, Germany
[b] Institute for Physical Chemistry and Electrochemistry, Leibniz University Hanover, Callinstr. 3-3A, D-30167 Hannover, Germany
[c] School of Chemistry & Chemical Engineering, South China University of Technology, 381 Wushan Road, 510640 Guangzhou, PR China

ARTICLE INFO

Article history:
Received 19 February 2008
Received in revised form
12 September 2008
Accepted 14 September 2008
Available online 20 September 2008

Keywords:
Perovskite
Membrane reactor
TAP
Mixed conductor
POM
ODE
Syngas

ABSTRACT

In order to identify factors governing selectivity of an oxygen-conducting perovskite $BaCo_xFe_yZr_zO_{3-\delta}$ (BCFZ) membrane in the partial oxidation of methane and ethane, mechanistic aspects of product formation in these reactions were investigated with a millisecond time resolution using the temporal analysis of products (TAP) reactor. It was found that the selectivity depends on: (i) reduction degree of the perovskite surface; the higher the reduction degree, the higher the ethane and ethylene selectivity in methane and ethane oxidation, respectively, and (ii) contact time; short contact times favor partial selective oxidation. The influence of contact time on the ethylene selectivity in ethane oxidation at degrees of ethane conversion above 85% was experimentally proven in hollow fiber and disk membranes, which differ in the contact times.

The low activity and selectivity in methane oxidation in the BCFZ perovskite membrane reactor were significantly increased, when the membrane on the hydrocarbon side was coated by a Ni-based steam reforming catalyst. This catalyst fulfils a double role: (i) it increases the oxygen transport through the perovskite membrane due to the high oxygen consumption, and (ii) it accelerates syngas production via deep methane oxidation followed by dry and steam reforming of methane. The syngas selectivity increases with an increase in the catalyst reduction degree, which is determined by the ratio of the rate of methane oxidation to the rate of oxygen permeation through the membrane.

1. Introduction

Due to the possibility to couple the chemical reaction and the separation of feed components and/or reaction products in one unit, membrane reactors are highly attractive to applications in several fields of modern science including biotechnology and chemical engineering [1,2]. Dense perovskite ceramic membranes exhibiting high oxygen ionic and electronic conductivity have drawn not only scientific but also industrial attention. These materials can easily separate oxygen from air and provide an economical source of oxygen without the drawback of any nitrogen ballast [1,2]. This type of oxygen transporting solids with coupled electron transfer is called mixed ion and electron conducting (MIEC) membrane. Such membranes have been successfully tested in the production of ethane/ethylene [3–6] and syngas (a mixture of CO and H_2) [7–11] from methane as well as in olefin production via oxidative dehydrogenation of alkanes [12–16]. In some cases the perovskite membrane itself served as a catalyst. The promising feature of MIEC membrane reactors is that the oxygen permeation flux can be tuned [17] enabling the control of selective and non-selective oxidation pathways. The number of potential applications of the MIEC membranes continuously grows. However, mechanistic studies of the ongoing catalytic reactions are scare. Usually, mechanistic knowledge derived from conventional catalytic tests is applied to membrane reactors with the aim to find out optimal reaction conditions for their operation. However, for oxidation reactions, the reaction mechanism may depend on the presence and absence of gas-phase oxygen. In this case, the effective optimization of the operation of membrane reactors requires additional studies on the mechanism and the kinetics under conditions similar to those in membrane reactors. Transient techniques are very useful for these purposes, because they permit to study individual reaction pathways, i.e. complex reaction networks can be unraveled in terms of near-to-elementary reaction steps.

The aim of the present study is to identify factors, which influence the selectivity of an oxygen-conducting perovskite $BaCo_xFe_yZr_zO_{3-\delta}$ (BCFZ) membrane in the partial oxidation of methane and ethane to syngas and ethylene, respectively. To this

* Corresponding author.
E-mail address: Evgenii.Kondratenko@catalysis.de (E.V. Kondratenko).

1381-1169/$ – see front matter © 2008 Elsevier B.V. All rights reserved.
doi:10.1016/j.molcata.2008.09.015

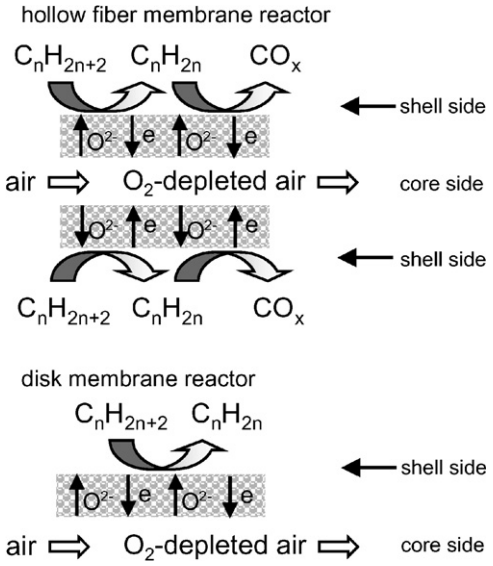

Fig. 1. Schematic representation of perovskite hollow fiber and disk membrane reactors for selective oxidation of hydrocarbons.

end, transient studies in the temporal analysis of products (TAP) reactor were combined with steady-state catalytic tests at ambient pressure. The mechanistic transient analysis was performed over $BaCo_xFe_yZr_zO_{3-\delta}$ and over a commercial Ni-based steam reforming (SR) catalyst supplied by Süd Chemie AG. For steady-state tests, the BCFZ membrane was used in a hollow fiber geometry, which was developed in the CaMeRa (Catalytic Membrane Reactor) project under the auspices of ConNeCat (Competence Network Catalysis) of the German Federal Ministry of Education and Research (BMBF).

2. Experimental

2.1. Oxidation in membrane reactors

The BCFZ perovskite hollow fiber membrane, which has been successfully used for the continuous oxygen separation from air [18–20], has been applied to the partial oxidation of methane and ethane. The experimental setup for catalytic tests in the membrane reactors using dense hollow fiber and disk membranes is schematically shown in Fig. 1. More details are described in Refs. [14,19,20]. Hydrocarbon (methane or ethane) diluted with helium was fed (40 mL/min–80 mL/min) to the shell side of the hollow fiber, while air was fed to the core side at a flow rate of 150 mL/min. The reaction temperature was varied from 700 to 925 °C. The feed and reaction components were analyzed by an online gas chromatograph (GC-Agilent 6890) equipped with two auto valves and Carboxen 1000 column (Supelco). The amount of H_2O was calculated from the hydrogen atom balance.

2.2. Transient experiments in the temporal analysis of products reactor

Transient analysis of CH_4 and C_2H_6 oxidation over the $BaCo_xFe_yZr_zO_{3-\delta}$ perovskite membrane (BCFZ, $x+y+z=1$ with δ as the oxygen non-stoichiometry, $0<\delta<1$) as well as over a Ni-based SR catalyst was performed in the TAP-2 reactor located in Berlin [21]. The TAP-2 reactor system has been thoroughly described in Ref. [22]. The Ni-based SR catalyst (85 mg) was used as received and without any treatment. The perovskite membrane was ground and pressed. Thereafter, the pressed perovskite was crashed and sieved to get particles of a size of 250–350 μm. 140 mg of these membrane particles were used for transient experiments. The catalytic materials were packed between two layers of quartz particles of the same size in the micro reactor ($Ø_{in}$ = 6 mm, length = 40 mm) made of quartz. Before transient experiments, the perovskite was pre-treated at ambient pressure in an O_2 flow (30 mL/min) at 875 °C for 1 h. After this oxidative treatment, the perovskite was exposed to vacuum (ca. 10^{-5} Pa) as required for transient experiments. The strong loss of oxygen observed upon the exposure of the catalyst to vacuum was recovered by O_2 pulsing at 875 °C and 800 °C before CH_4 and C_2H_6 pulsing, respectively. Thereafter, multi-pulse experiments with CH_4 and C_2H_6 were started. In these experiments, a mixture of CH_4:Ne = 1:1 or C_2H_6:Ne = 1:1 was repeatedly (ca. 900 pulses) pulsed over the treated perovskite and the Ni-based SR catalyst. The pulse size was ca. 4×10^{15} and 2×10^{16} molecules in the experiments with CH_4 and C_2H_6, respectively.

In order to unravel origins of CO and H_2 formation in the partial oxidation of methane over the Ni-based SR catalyst, not only CH_4–O_2 but also CH_4–CO_2 interactions were studied. In these experiments CH_4:O_2:Ne = 2:1:2 and $^{13}CH_4$:$^{12}CO_2$:Ne = 1:1:1 mixtures were pulsed at 800 °C. The influence of oxygen coverage on the CO_2 reforming of CH_4 was studied at 800 °C in a sequential pulse mode using O_2:Xe = 1:1 and $^{13}CH_4$:$^{12}CO_2$:Ne = 1:1:1 mixtures.

A quadrupole mass spectrometer (HAL RC 301 Hiden Analytical) was used for quantitative analysis of reactants and reaction products. The following atomic mass units (AMUs) were used for mass-spectroscopic identification of different compounds: 60 (CH_3COOH), 45 (CH_3COOH, C_2H_5OH), 44 (CH_3CHO, CO_2), 43 (CH_3COOH), 31 (C_2H_5OH, CH_3OH), 30 (C_2H_6), 29 (C_3H_8, C_2H_5OH, CH_3CHO, C_2H_6), 28 (C_3H_8, C_2H_6, C_2H_4, CO_2, CO), 27 (C_3H_8, C_3H_6, C_2H_6, C_2H_4), 26 (C_2H_6, C_2H_4), 20 (Ne), 18 (H_2O) and 2 (H_2). For multi-pulse experiments, the individual AMU's were recorded without averaging. Otherwise, pulses were repeated 10 times for each AMU and averaged to improve the signal-to-noice ratio. The concentration of feed components and reaction products was determined from the respective AMUs using standard fragmentation patterns and sensitivity factors.

3. Result and discussion

The results of continuous-flow oxygen-free conversion of methane and ethane in the BCFZ membrane reactor in the absence and the presence of a commercial Ni-based steam reforming catalyst are described and discussed in Section 3.1. Section 3.2 deals with the transient analysis of C_2H_4, C_2H_6 and CO_x formation from CH_4 and C_2H_6 over a bare BCFZ perovskite. Then, the origins of CO and H_2 formation in CH_4 conversion with O_2 and CO_2 over the Ni-based SR catalyst are discussed in Section 3.3. Finally (Section 3.4), the fundamental mechanistic knowledge derived is used for optimizing catalytic performance of the BCFZ membrane reactor for oxidative conversions of methane and ethane to syngas and ethylene, respectively.

3.1. Oxidation of methane and ethane in BCFZ membrane reactor

3.1.1. Performance of bare BCFZ membrane reactor

Continuous-flow oxidation of methane and ethane was studied in the perovskite hollow fiber membrane reactor schematically shown in Fig. 1. In this reactor, the hydrocarbon and air flows were separated by the BCFZ membrane. CO_2 was identified as the only carbon-containing product of CH_4 oxidation at 875 °C (Fig. 2(a)). Neither aromatics nor carbon deposition were detected. The absence of coke deposition may be due to the fact that the coke formed was continuously oxidized by oxygen permeated through the membrane from the air side to the shell one. The overall flow

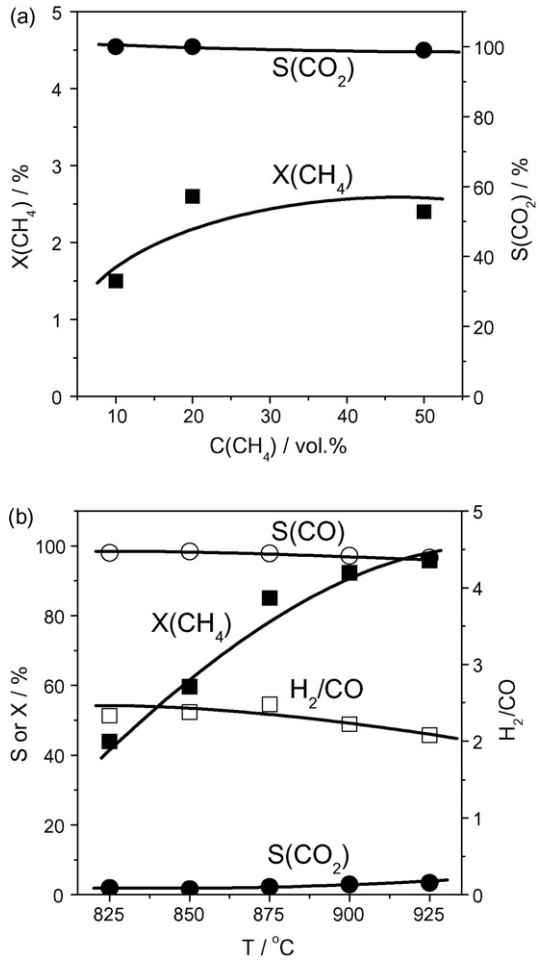

Fig. 2. Catalytic performance of the BCFZ hollow fiber membrane reactor in methane oxidation without (a) and with (b) Ni-based steam reforming catalyst (Süd Chemie AG). Experimental conditions for (a): air flow rate on the shell side: 150 ml/min, total flow rate on the core side: 30 ml/min with 10–50 vol.% CH_4, membrane surface area: 3.3 cm^2, T = 875 °C. Experimental conditions for (b): air flow rate on the core side: 150 ml/min, total flow rate of on the shell side: 20 ml/min with 50 vol.% methane, membrane surface area: 0.56 cm^2, catalyst amount: 0.4 g, T = 825–925 °C.

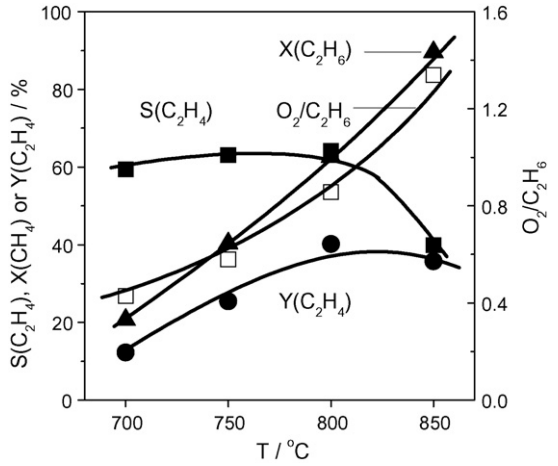

Fig. 3. Effect of temperature on ethane conversion and product selectivity in the BCFZ hollow fiber membrane reactor. Experimental conditions: flow rate on the core side: 40 mL/min of a mixture of 10 vol.% ethane and 90 vol.% He, air flow rate on the shell side: 300 mL/min, membrane surface area: 3.52 cm^2.

of O_2 permeated was about 6.8 ml/min. However, only 5–10% of O_2 reacted with CH_4. The methane conversion did not exceed 3%. Such a low degree of methane conversion in the presence of large amounts of un-reacted O_2 is surprising. Taken these results into account, it is concluded that although the perovskite membrane effectively transported oxygen from the air side to the hydrocarbon side it showed the low intrinsic activity for methane oxidation. Moreover, the low methane conversion indicates that gas-phase methane oxidation with oxygen was slow as well at this temperature. The above results point out that the rate of oxygen transport through the membrane including desorption of gas-phase O_2 is faster than methane oxidation. This important conclusion together with the mechanistic results from Sections 3.2 and 3.3 is very essential for optimizing the reactor performance as discussed in Section 3.4.

In contrast to the methane oxidation (Fig. 2(a)), ethane is selectively converted to ethylene over the BCFZ membrane without any additional catalyst and oxygen co-feeding in the temperature range from 700 to 850 °C (Fig. 3). When reaction temperature increases from 700 to 800 °C, the ethane conversion and ethylene selectivity increase from 21 to 63% and from 59 to 64%, respectively. This is unusual for ethane oxidation to ethylene, since the ethylene selectivity typically decreases with increasing ethane conversion [23]. However, the ethylene selectivity drops from 60 to 40%, while the ethane conversion increased from 60 to 90%, when the reaction temperature was further increased up to 850 °C (Fig. 3). Such a strong decrease in the ethylene selectivity may be explained as follows. Upon increasing the degree of ethane conversion from 60 to 90%, the outlet ethane concentration decreases from 4 to 1 vol.% and becomes similar to that of ethylene (0.36 vol.%). Due to the higher chemical activity of ethylene as compared to ethane, ethylene combustion starts to overcome ethylene formation from ethane. Another factor, which can also contribute to the drop of the ethylene selectivity, is the temperature-induced intensification of oxygen transport through the perovskite membrane to the hydrocarbon side resulting in an increase in the ratio of O_2/C_2H_6 from 0.85 to 1.35 with increasing reaction temperature from 800 to 850 °C (Fig. 3). The oxygen permeation flux was calculated from the flows of non-reacted oxygen and reaction products containing oxygen on the shell side of the membrane. Generally, high oxygen partial pressure is more favorable for the total oxidation than for the selective dehydrogenation.

3.1.2. *Performance of the BSFZ membrane reactor in the presence of Ni-based SR catalyst*

As shown above, the BCFZ membrane has low activity for methane oxidation at 850 °C, although it effectively transports oxygen from the air side to the hydrocarbon side. Therefore, it is reasonable to combine the membrane with a suitable catalyst to selectively oxidize methane with gas-phase oxygen permeated through the membrane. To this end, a Ni-based steam reforming catalyst was deposited on the hydrocarbon side of the membrane. Fig. 2(b) exemplifies the catalytic performance of the BCFZ membrane reactor in the presence of this catalyst at different temperatures. The two key effects of the Ni-based catalyst on the performance of the membrane reactor should be especially highlighted: (i) methane conversion increases from ca. 3% to ca. 60% at 850 °C; (ii) CO and H_2 become the main reaction products; the CO selectivity exceeds 95% and the H_2/CO ratio is ca. 2. These noteworthy changes in the catalytic performance evidence that the methane conversion occurs mainly over the Ni-based SR catalyst. The role of the perovskite membrane is restricted to the oxygen transport from the air side to the hydrocarbon side. A near to complete methane conversion was achieved, when the reaction temperature was increased up to 925 °C. However, the CO selectivity slightly

dropped in favor of CO_2 (Fig. 2(b)). A similar effect was also reported for methane oxidation in an $YBa_2Cu_3O_{7-x}$ membrane reactor with a Ni/ZrO_2 catalyst [24]. On the other hand, when methane and oxygen were together fed to fluidized-bed [25,26] and fixed-bed [27,28] reactors filled with Ni-based catalysts, the CO selectivity increased continuously with temperature. In order to identify possible origins of CO selectivity drop in the membrane reactors in contrast to the reactors operating with co-fed CH_4 and O_2, factors governing the selectivity of methane oxidation to syngas were analyzed by transient analysis of products (Section 3.3).

3.2. Mechanistic aspects of CH_4 and C_2H_6 oxidation over bare BCFZ perovskite

Mechanistic insights into the reaction pathways of products formation in CH_4 and C_2H_6 oxidation over the BCFZ perovskite were derived from the CH_4 and C_2H_6 pulse experiments performed in the TAP reactor. In agreement with the results of catalytic tests in the membrane reactor (Section 3.1), CO_2 was identified as the main reaction product of methane oxidation in the TAP reactor. However, C_2H_6 was also detected upon CH_4 pulsing. The presence of C_2H_6 in the TAP experiments in contrast to the experiments in the membrane reactor can be due to the significantly shorter contact times (millisecond range) in the TAP reactor. Therefore, the primarily formed C_2H_6 was not completely oxidized to CO_2 in contrast to catalytic tests in the membrane reactor. In addition to CO_2 and C_2H_6, surface carbon-containing deposits were also formed as concluded from carbon balance (~50%).

CO_2 formation dominated also, when a C_2H_6:Ne = 1:1 mixture was pulsed over the oxidized BCFZ perovskite at 800 °C. Additionally to CO_2, C_2H_4 was observed, however, as a minor product. The carbon balance in the C_2H_6 pulse experiments was not lower than 80% indicating lower formation of carbon deposits from C_2H_6 as compared to CH_4. This may be due to lower reaction temperature in the case of C_2H_6. Since gas-phase oxygen was not present in the CH_4 and C_2H_6 pulse experiments, lattice oxygen of the BCFZ perovskite must be responsible for the formation of selective and non-selective reaction products. The presence of C_2H_6 and C_2H_4 in the CH_4 and C_2H_6 pulse experiments proved the ability of the BCFZ perovskite to catalyze the oxidative coupling of methane (OCM) and the oxidative dehydrogenation of ethane (ODE), respectively.

In order to identify the origins of selective and non-selective reaction products, the shape and the order of appearance of feed components and reaction products were analyzed. These characteristics contain information about the sequence of product formation from feed components [22]. The transient responses of CH_4, C_2H_6, C_2H_4, and CO_2 were normalized by their height for better comparing their characteristic. The normalized transients are presented in Fig. 4. For methane oxidation, the narrow shape of the CH_4 transient indicates irreversible consumption of CH_4, i.e. its oxidation. The transient response of C_2H_6 is shifted to longer times and is slightly broader than the CH_4 transient. This means that C_2H_6 is formed from CH_4. In contrast to the transient responses of CH_4 and C_2H_6, CO_2 gives a very broad signal shifted to considerably longer times.

The CO_2 transient response formed upon C_2H_6 pulsing over the oxidized BCFZ perovskite at 800 °C (50 °C lower than in the CH_4 pulse experiments) is also significantly broader and shifted to longer times as compared to C_2H_6 and C_2H_4 (Fig. 4). The C_2H_4 transient response is similar to the C_2H_6 one but shifted to slightly longer times. Based on the order of appearance of feed components and reaction products it can be postulated that CH_4 and C_2H_6 are primarily converted to C_2H_6 and C_2H_4, respectively. CO_2 stems mainly via consecutive oxidation of these primarily formed products. This statement agrees well with the results in Refs. [23,29].

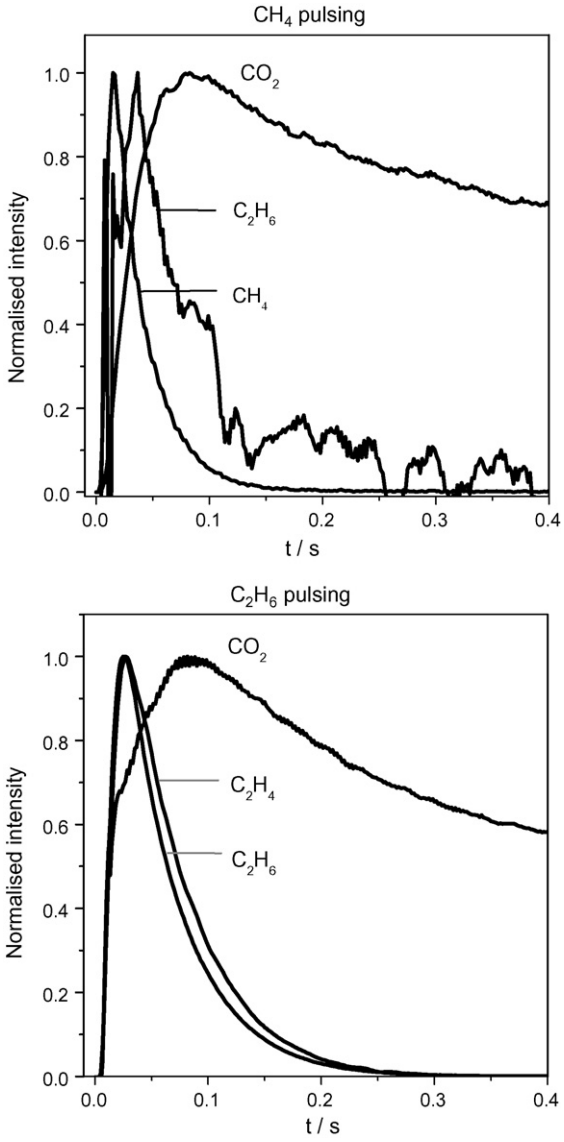

Fig. 4. Height-normalised transient responses of CH_4, C_2H_6 and CO_2 obtained after pulsing of a CH_4:Ne = 1:1 mixture and height-normalised transient responses of C_2H_6, C_2H_4 and CO_2 obtained after pulsing of a C_2H_6:Ne = 1:1 mixture over the oxidised BCFZ perovskite (m = 0.140 g) at 875 °C (for CH_4) and 800 °C (for C_2H_6) in the TAP reactor.

Moreover, it is also supported by the activity order of hydrocarbon oxidation: $C_2H_4 > C_2H_6 > CH_4$. However, it is not possible to unambiguously exclude CO_2 formation via direct CH_4 or C_2H_6 oxidation, since the shift of the CO_2 transient signal and its very broad shape can be also attributed to the strong adsorption of CO_2 over BaO followed by its retarded desorption. The below analysis of CH_4 and C_2H_6 multi-pulse experiments further supports that CO_2 is a secondary product in CH_4 and C_2H_6 oxidation over oxidized BCFZ perovskite in the absence of gas-phase oxygen.

The participation of lattice oxygen species in the selective oxidation of hydrocarbons opens an attractive possibility for the process optimization in the membrane reactor. The reduction degree of perovskite surface on the hydrocarbon site can be tuned by adjusting partial pressure of the hydrocarbon on the hydrocarbon site or/and by the oxygen partial pressure on the air side. The correlation between the reduction degree of the catalyst and respective product distribution can be easily established from CH_4 and C_2H_6 multi-pulse experiments in the TAP reactor. In these experiments,

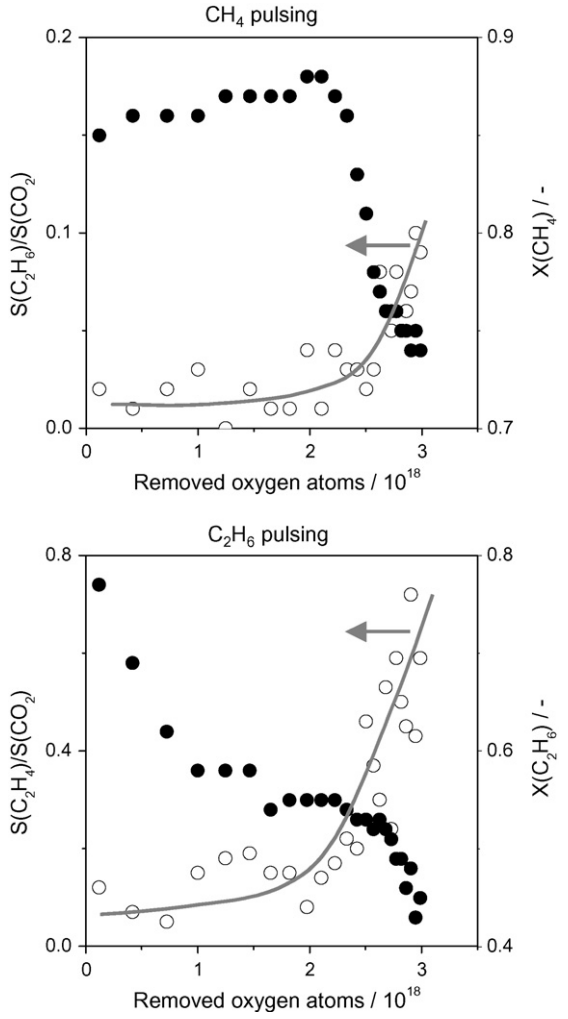

Fig. 5. Selectivity ratios of $S(C_2H_6)/S(CO_2)$ and $S(C_2H_4)/S(CO_2)$ as well as CH_4 and C_2H_6 conversion versus the amount of oxygen removed from the BCFZ perovskite after pulsing of a CH_4:Ne = 1:1 mixture at 875 °C and a C_2H_6:Ne = 1:1 mixture at 800 °C, respectively, in the TAP reactor.

oxygen species are continuously removed from the catalyst lattice as oxygen-containing products of hydrocarbon oxidation. The hydrocarbon multi-pulse experiments performed in the present study consisted of ca. 900 pulses with a pulse intensity of 4×10^{15} and 2×10^{16} molecules of CH_4 and C_2H_6, respectively. In the following, we analyze the dependence of product distribution on the amount of oxygen removed from the perovskite in the CH_4 and C_2H_6 multi-pulse experiments. This amount was calculated from the amount of reaction products considering the stoichiometry of their formation given by Eqs. (1)–(4). Thus, one lattice oxygen is required for selective oxidation of CH_4 and C_2H_6 (Eqs. (1) and (3)), while 4 or 7 oxygen atoms are required for CO_2 formation from CH_4 (Eq. (2)) and C_2H_6 (Eq. (4)), respectively.

$$CH_4 + O \rightarrow C_2H_6 + H_2O \quad (1)$$

$$CH_4 + 4O \rightarrow CO_2 + 2H_2O \quad (2)$$

$$C_2H_6 + O \rightarrow C_2H_4 + H_2O \quad (3)$$

$$C_2H_6 + 7O \rightarrow 2CO_2 + 3H_2O \quad (4)$$

The continuous removal of lattice oxygen from the catalyst upon pulsing of CH_4 or C_2H_6 results in a consistent increase in the degree of perovskite reduction. Fig. 5 nicely shows an increase in the selectivity ratio of $S(C_2H_6)/S(CO_2)$ in CH_4 oxidation and the selectivity ratio of $S(C_2H_4)/S(CO_2)$ in C_2H_6 oxidation with an increasing amount of lattice oxygen removed from the perovskite. In other words, the selective reactions (OCM and ODE) are favored by an increased reduction degree of the perovskite. Not only the product distribution but also the degree of hydrocarbon conversion is influenced by the reduction degree of the BSCF membrane; the higher the number of oxygen removed, the lower the hydrocarbon conversion. This is an important result, because the dependence of product selectivity on conversion of feed components provides direct experimental insights into the sequence of product formation. Since the ratios of $S(C_2H_6)/S(CO_2)$ in CH_4 oxidation and of $S(C_2H_4)/S(CO_2)$ in C_2H_6 oxidation increase with a decrease in the degree of hydrocarbon conversion (Fig. 5), it can be concluded that CO_2 originates via consecutive oxidation of primarily formed C_2H_6 and C_2H_4, respectively. If CO_2 would be directly formed from feed components, the above selectivity ratios should not depend on the degree of hydrocarbon conversion.

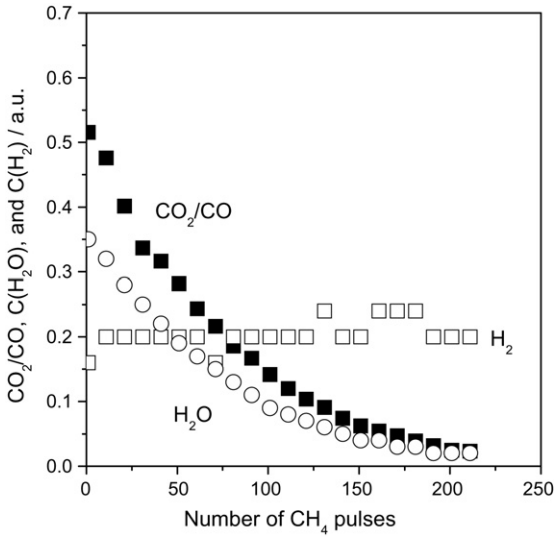

Fig. 6. The ratio of concentrations of CO_2/CO, as well as the concentrations of H_2O, and H_2 versus the number of CH_4 pulses (CH_4:Ne = 1:1) over Ni-based steam reforming catalyst (Süd Chemie AG) at 800 °C. Pulse size of CH_4 is ca. 10^{16} molecules.

Thus, the transient experiments with CH_4 and C_2H_6 have shown that: (i) lattice oxygen of the BCFZ perovskite is active and selective for CH_4 and C_2H_6 oxidation to C_2H_6 and C_2H_4, respectively; (ii) CH_4, C_2H_4 and C_2H_6 compete for the same lattice oxygen species; (iii) CO_x is mainly formed via consecutive oxidation of selective products of methane and ethane oxidation.

3.3. Mechanistic insights into CO and H_2 formation over Ni-based SR catalyst

When CH_4 was pulsed over a non-reduced Ni-based steam reforming catalyst, CO, CO_2, H_2O, and H_2 were detected at the reactor outlet. The presence of oxygen-containing products proves the ability of lattice oxygen of nickel oxide to oxidize methane. Fig. 6 shows that the CO_2/CO ratio and the H_2O concentration decrease with an increasing number of CH_4 pulses. These changes in the catalytic performance can be explained as follows. Fresh catalyst possesses NiO that is active for total oxidation of CH_4 to CO_2. Upon removing lattice oxygen from NiO as CO_2 and H_2O, the degree of the catalyst reduction increases, i.e. this process leads to a partial reduction of NiO to Ni^0. The latter is selective for CO formation [30]. Therefore, partial methane oxidation to CO starts to prevail over the total methane oxidation to CO_2.

In contrast to the formation of CO, CO_2, and H_2O, the H_2 production did not depend on the number of CH_4 pulses. The distinct dependence of the CO_2/CO ratio and of H_2 concentration on the number of CH_4 pulses (Fig. 6) indicates that CO and H_2 are not formed via the same reaction pathways. In order to identify the reaction pathways leading to syngas, the transient responses obtained during CH_4 pulsing over the Ni-based SR catalyst at 800 °C were analyzed. To this end, the time scale of the transients of methane and products of its oxidation were normalized according to Ref. [22]. However, in contrast to the literature [22], we have applied a three-zone reactor. We considered the diffusion of feed molecules through the whole reactor but the diffusion of reaction products from the beginning of the catalyst bed. This normalization makes it possible to compare the order of the appearance of gas-phase components, which differ significantly in their molecular weights, i.e. H_2, CO, and CO_2. The normalized transient responses of CH_4, CO_2, CO, and H_2 are shown in Fig. 7. The CH_4 response is the narrowest one and shifted to the shortest normalized time. These characteristics evidence that methane is consumed, i.e. reacts with lattice oxygen of the catalyst, since no gas-phase O_2 was present in the CH_4 pulses. For identifying the order of product formation from methane, the dimensionless times of maximal concentration (t_{max}) of CO_2, CO, and H_2 were calculated. The CO_2 transient response is characterized by the t_{max} of 3.089, while the t_{max} of CO and H_2 are 4.658 and 5.187, respectively. The t_{max} of CH_4 is significantly shorter than those of the reaction products and amounts to 0.5. Based on the t_{max} values and the width of transient responses, it is concluded that CH_4 is primarily converted to CO_2 followed by its conversion to CO.

When a CH_4:O_2:Ne = 2:1:2 mixture was pulsed over the Ni-based SR catalyst at 800 °C no changes in the order of the t_{max} of CH_4, CO_2, CO, and H_2 were observed as compared to single CH_4 pulse experiments (Fig. 7). Therefore, it can be suggested that in a similar manner to the CH_4 oxidation by lattice oxygen, CO_2 is the primary product of CH_4 oxidation in the presence of gas-phase O_2. The primarily formed CO_2 is consecutively transformed to CO. However, the absolute values of all the t_{max} decreased significantly. This means that oxygen accelerates not only the methane conversion to CO_2 but also the formation of CO and H_2.

$$t_{max}^{CH_4}(0.438) < t_{max}^{CO_2}(1.738) < t_{max}^{CO}(2.239) < t_{max}^{H_2}(3.65)$$

In order to support or reject the above conclusion, methane and carbon dioxide interactions were also investigated by pulsing a $^{13}CH_4$:$^{12}CO_2$:Ne = 1:1:1 mixture. The application of labeled $^{13}CH_4$ is essential for independent monitoring the transformations of labeled methane and non-labeled carbon dioxide. $^{13}CO_2$, ^{13}CO, $^{12}CO_2$, ^{12}CO, and H_2 were observed as reaction products. The order of the t_{max} of the feed components and the reaction products in this experiment is:

$$t_{max}^{^{12}CO_2}(0.886) < t_{max}^{^{13}CH_4}(1.157) < t_{max}^{^{13}CO_2}(2.004) < t_{max}^{^{12}CO}(2.735) < t_{max}^{^{12}CO}(3.146) < t_{max}^{H_2}(3.586)$$

Among ^{13}C-containing components, $^{13}CH_4$ has the lowest t_{max} followed by those of $^{13}CO_2$ and ^{13}CO. Based on this order, it can be formally concluded that $^{13}CH_4$ is primarily converted to $^{13}CO_2$. Direct methane oxidation to carbon dioxide has been earlier observed in $^{12}CO_2$ reforming of $^{13}CH_4$ over Ni-La_2O_3/Zeolite 5A [31] and Ni/SiO_2 [32] between 600 and 800 °C. The higher t_{max} value of ^{13}CO as compared to that of $^{13}CO_2$ indicates that the latter is an intermediate in ^{13}CO formation. This conclusion is supported by the presence of ^{12}CO, which is formed from the fed $^{12}CO_2$. The following reaction pathways are suggested to be responsible for the conversion of CO_2 to CO: (i) direct CO_2 decomposition, (ii) interac-

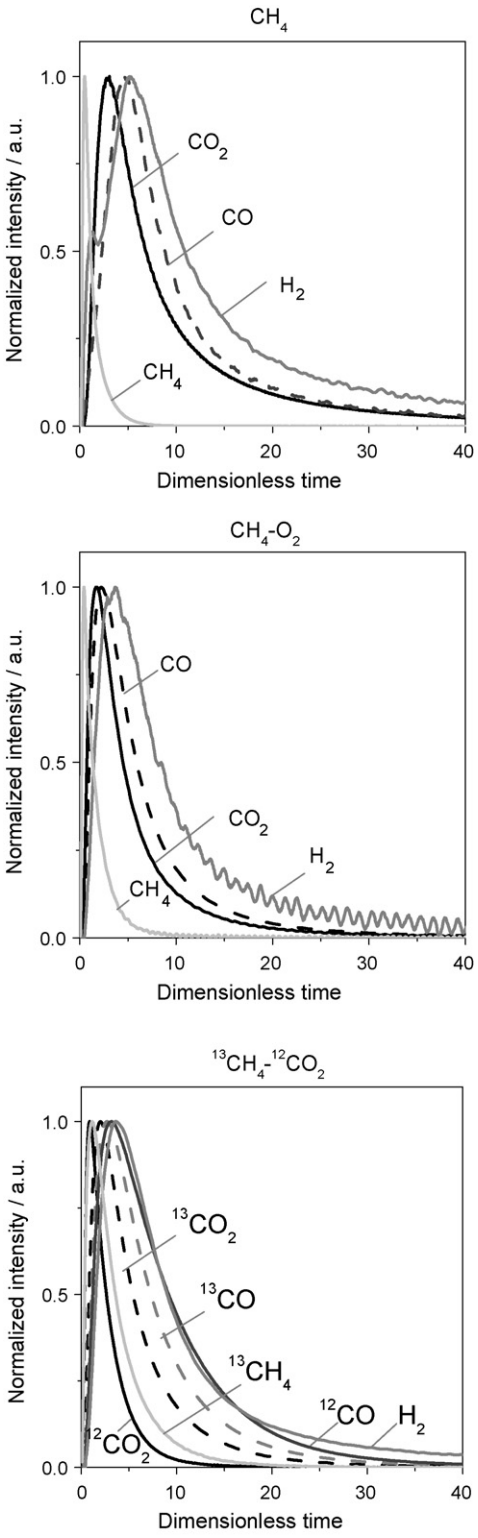

Fig. 7. Normalized transient responses of the reaction products obtained after pulsing of CH_4 (CH_4:Ne = 1:1), and CH_4-O_2 (CH_4:O_2:Ne = 2:1:2) and $^{13}CH_4$-$^{12}CO_2$ ($^{13}CH_4$:$^{12}CO_2$:Ne = 1:1:1) mixtures over Ni-based steam reforming catalyst (Süd Chemie AG) at 800 °C.

tion of CO_2 with carbon deposits, and (iii) reaction between CO_2 and adsorbed CH_x species described by Eq. (5). Cui et al. [33] have reported that the reaction between methane fragments and CO_2 is slower than methane dissociation, being the rate limiting step of the CO_2 reforming of CH_4 between 650 and 750 °C. Based on the latter statement it can be assumed that the contribution of this reaction to the total CO and H_2 formation, therefore, causes the observed broadening of the transient responses of CO and H_2.

$$CH_{x,surface} + CO_2 + (x+1)_{surface} \rightarrow 2CO_{surface} + xH_{surface} \quad (5)$$

For elucidating the role of oxygen in the dry reforming of methane, sequential pulse experiments were performed with O_2:Xe = 1:1 and $^{13}CH_4$:$^{12}CO_2$:Ne = 1:1:1 mixtures pulsed with a time delay of 0.2 s between the mixtures. Oxygen was completely consumed in the O_2 pulse, while neither ^{13}CO nor ^{12}CO was observed in the $^{12}CO_2$–$^{13}CH_4$ pulse. The only C-containing gas-phase product was $^{13}CO_2$ indicating total combustion of methane. Taking into account the complete consumption of pulsed O_2, the absence of carbon monoxide can be explained as follows. Metallic Ni^0 is oxidized to NiO in the O_2 pulse. Since the $^{13}CH_4$-contatining mixture entered the reactor after the O_2 pulse, methane reacted with NiO yielding carbon dioxide as found in Ref. [30]. From a mechanistic point of view, CO_2 does not effectively decompose to CO over oxidized Ni species. Moreover, the high coverage by oxygen species hinders the CO formation via interaction of CO_2 with surfaced CH_x fragments due to their rapid oxidation. This mechanistic knowledge is highly important for optimizing the methane oxidation in membrane reactors as discussed below.

3.4. Fundamental approaches for optimizing catalytic performance of BCFZ membrane reactor for oxidative CH_4 and C_2H_6 utilization

As our above mechanistic analysis of CH_4 and C_2H_6 oxidation over the BCFZ membrane predicts, the reduction degree of the membrane is one of the selectivity-determining factors; high reduction degree of the membrane is favorable for selective methane and ethane transformations like OCM and ODE. Taking into account the present and previous results [34], it can be concluded that the following reaction pathways control the reduction degree of the membrane: (i) reaction of lattice oxygen with hydrocarbons (Eq. (6)), (ii) formation of gas-phase oxygen (Eq. (7)), and (iii) diffusion of lattice oxygen through the membrane (Eq. (8)).

$$C_nH_{2n+2} + O_s{}^{2-} \rightarrow C_2H_{2n} + CO_x + H_2O \quad (6)$$

$$O_s{}^{2-} \rightarrow \frac{1}{2}O_2 + 2\bar{e} \quad (7)$$

$$O_s{}^{2-}(\text{air side}) \rightarrow O_s{}^{2-}(\text{hydrocarbon side}) \quad (8)$$

The reaction described by Eq. (7) takes place if the lattice oxygen of the perovskite membrane is not completely consumed due to the low reaction rate of alkane oxidation as compared to the diffusion rate of lattice oxygen through the membrane (Eq. (8)). Since the latter reaction is more strongly influenced by temperature than the former, the reduction degree of the membrane is, unfortunately, low at high temperatures, at which economically attractive high space–time yields of products of alkane oxidation can be achieved. Therefore, above 850 °C deep oxidation reactions are more favored than the OCM and ODE. Due to the higher reactivity of ethane as compared to methane, the ODE reaction can be selectively performed at lower temperatures but not at a complete ethane conversion. Therefore, the challenge in selective hydrocarbon oxidation using the BCFZ membrane is to suppress the non-selective oxidation reactions at high oxygen fluxes.

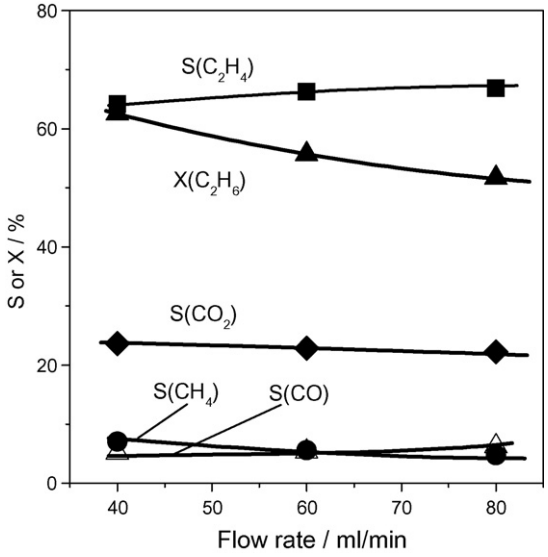

Fig. 8. Influence of flow rate of a 10:90 = C_2H_6:He mixture on ethane conversion and product selectivity in the BCFZ perovskite hollow fiber membrane reactor at 800 °C. Membrane surface area: 3.52 cm^2, air flow rate on the shell side: 300 mL/min.

As shown in Section 3.2 ethane and ethylene compete for lattice oxygen of the perovskite membrane, and the consecutive ethylene oxidation is the main source of CO_x. Therefore, a high ethylene selectivity can be achieved only when ethylene is removed from the reaction zone before it is further combusted, for example, by a decrease in the contact time. This approach was proven by performing ethane oxidation at different contact times using the BCFZ hollow fiber membrane reactor (Fig. 1). The results obtained are summarized in Fig. 8. As expected, the ethylene selectivity increased but, unfortunately, the ethane conversion decreased, when ethane flow rate was increased. Another possibility to avoid consecutive ethylene oxidation with high ethane conversion kept is to optimize the geometry of the membrane reactor. In the present study, hollow fiber membrane and disk membrane reactors were applied (Fig. 1). The ethylene selectivity in the latter reactor was ca. 80% as compared to only 40% in the former one at ethane conversion of ca. 90% (Table 1). The high ethylene yield and selectivity obtained in the disk membrane reactor are comparable with those reported in literature. An ethylene yield of 56% with an ethylene selectivity of 80% was achieved in a dense tubular ceramic membrane reactor made of $Bi_{1.5}Y_{0.3}SmO_3$ at 875 °C [12]. Wang et al. [13,14] reported an ethylene selectivity of 80% at an ethane conversion of 84% at 800 °C using planar and tubular oxygen permeable mixed ion and electron-conducting membranes made of $Ba_{0.5}Sr_{0.5}Co_{0.8}Fe_{0.2}O_{3-\delta}$. On the same material an ethylene yield of 66% was obtained at 807 °C and could be improved up to 76% after Pd deposition [16].

Unfortunately, the above approach is not appropriate for the OCM reaction in the BCFZ perovskite membrane reactor due to the considerably lower reactivity of methane as compared to ethane

Table 1
Catalytic performance of BCFZ disk membrane and BCFZ hollow fiber membrane reactors in the oxidative dehydrogenation of C_2H_6 to C_2H_4 at 800 °C. Experimental details: membrane surface area of disk membrane and hollow fiber are 0.90 cm^2 and 3.52 cm^2, respectively; 10:90 = C_2H_6:He and air flow rates are 40 and 300 mL/min, respectively.

Reactor types	C_2H_6 conversion (%)	Product selectivity (%)			
		C_2H_4	CH_4	CO	CO_2
Disk membrane	85.2	79.1	10.7	5.4	4.8
Hollow fiber membrane	89.6	39.9	12.1	15.4	32.6

requiring temperatures above 850 °C, where oxygen flux is too high. An alternative is to combine the BCFZ perovskite membrane with a suitable catalyst, which converts methane to useful reaction products. In the present study, a Ni-based SR catalyst was used for coating of the BCFZ membrane. As a result, the performance of the perovskite hollow fiber membrane reactor has been significantly changed (Fig. 2); instead of deep oxidation without the SR catalyst, methane is selectively converted to syngas in the presence of this catalyst. Besides the syngas production, the catalyst increases the oxygen flux through the membrane by an improved oxygen conversion on the hydrocarbon side thus promoting the driving force for oxygen permeation according to the Wagner [35] equation (Eq. (9)).

$$\text{Flux}(O_2) \sim \frac{p_{O_2(\text{air side})}}{p_{O_2(\text{hydrocarbon side})}} \quad (9)$$

However, it should be noted that the excess of oxygen on the catalyst surface negatively influences syngas production as shown in Section 3.3. From a practical point of view, this means that the methane and oxygen flows should be optimized to ensure high methane conversion at a near to complete oxygen consumption.

Summarizing the above discussion, it is concluded that selective oxidation of methane or ethane in oxygen-conducting membrane reactors should be performed at temperatures, where the rate of hydrocarbon oxidation is higher than the rate of oxygen transport through the membrane. Moreover, it is highly important to optimize the geometry of the membrane for ensuring short contact times favoring selective oxidation over non-selective combustion. The catalytic performance can be also improved in the presence of a catalyst over the hydrocarbon side of the membrane, which selectively operates in the presence of gas-phase O_2.

4. Conclusions

The mechanism of methane and ethane oxidation over the BCFZ perovskite and the Ni-based steam reforming catalyst has been elucidated in the TAP reactor. For both hydrocarbons, lattice oxygen of the perovskite is responsible for their conversion to C_2H_6 and C_2H_4 in the oxidative coupling of methane and in the oxidative dehydrogenation of ethane, respectively. These selective reaction products compete with the feed hydrocarbons for the same lattice oxygen species but produce deep oxidation products only. The latter reaction can be suppressed, when the degree of catalyst reduction is increased, and/or when the selective products are removed from the reaction zone. The latter concept was proven valid for ethane oxidation to ethylene. The disk membrane reactor was found to be more efficient in the ethane conversion than the hollow fibre membrane reactor due to its optimal geometry for achieving shorter contact times. However, this concept does not work for methane oxidation due to its high chemical inertness requiring high operation temperatures, where the ratio of fed methane to oxygen transported through the membrane is too low for selective methane oxidation. The efficiency of the perovskite membrane reactor could be enhanced by its combining with Ni-based steam reforming catalyst. In the presence of the catalyst, methane is almost completely converted to syngas (H_2 and CO) with ca. 95% selectivity via total methane oxidation followed by dry and steam reforming steps.

Acknowledgements

The perovskite hollow fiber membranes used were developed in the CaMeRa (Catalytic Membrane Reactor) project under the auspices of ConNeCat (Competence Network Catalysis) financed by the German Federal Ministry of Education and Research (BMBF). EVK thanks Deutsche Forschungsgemeinschaft (DFG) in the frame of the competence network (Sonderforschungsbereich 546) "Structure, dynamics and reactivity of transition metal oxide aggregates". HW greatly thanks the financial support from the Alexander von Humboldt Foundation. The authors thank Süd Chemie AG for providing the Ni-containing steam reforming catalysts.

References

[1] J.A. Dalmon, A. Giroir-Fendler, C. Mirodatos, H. Mozzanega, Catal. Today 25 (1995) 1.
[2] E. Drioli, D.R. Paul, Ind. Eng. Chem. Res. 46 (2007) 2235, and the following references in this volume.
[3] J.E. Elshof, H.J.M. Bouwmeester, H. Verweij, Appl. Catal. A 130 (1995) 195.
[4] Y.P. Lu, A.G. Dixon, W.R. Roser, Y.H. Ma, U. Balachandran, J. Membr. Sci. 170 (2000) 27.
[5] F.T. Akin, Y.S. Lin, AIChE 48 (2002) 2298.
[6] H.H. Wang, Y. Cong, W.S. Yang, Catal. Today 104 (2005) 160.
[7] C.Y. Tsai, A.G. Dixon, W.R. Moser, Y.H. Ma, AIChe J. 43 (1997) 2741.
[8] T. Ishihara, Y. Tsuruta, T. Todaka, H. Nishiguchi, Y. Takita, Solid State Ionics 152 (2002) 709.
[9] H.H. Wang, Y. Cong, W.S. Yang, Catal. Today 82 (2003) 157.
[10] H.J.M. Bouwmeester, Catal. Today 82 (2003) 141.
[11] M. Ikeguchi, T. Mimura, Y. Sekine, E. Kikuchi, M. Matsukata, Appl. Catal. A 290 (2005) 212.
[12] F.T. Akin, Y.S. Lin, J. Membr. Sci. 209 (2002) 457.
[13] H.H. Wang, Y. Cong, W.S. Yang, Chem. Commun. 14 (2002) 1468.
[14] H.H. Wang, Y. Cong, W.S. Yang, Catal. Lett. 84 (2002) 101.
[15] H.H. Wang, Y. Cong, X.F. Zhu, W.S. Yang, React. Kinet. Catal. Lett. 79 (2003) 351.
[16] M. Rebeilleau, A.C. van Veen, D. Farrusseng, J. Rousset, C. Mirodatos, Z.P. Shao, G.X. Xiong, Stud. Surf. Sci. Catal. 147 (2004) 655.
[17] P.J. Gellings, H.J.M. Bouwmeester, Catal. Today 12 (1992) 1.
[18] H.H. Wang, S. Werth, T. Schiestel, J. Caro, Angew. Chem. Int. Ed. 44 (2005) 2.
[19] T. Schiestel, M. Kilgus, S. Peter, K.J. Caspary, H.H. Wang, J. Caro, J. Membr. Sci. 258 (2005) 1.
[20] C. Tablet, G. Grubert, H.H. Wang, T. Schiestel, M. Schroeder, B. Langanke, J. Caro, Catal. Today 104 (2005) 126.
[21] http://www.catalysis.de/Transient-mechanistic-studies.412.0.html?&L=1.
[22] J.T. Gleaves, G.S. Yablonskii, P. Phanawadee, Y. Schuurman, Appl. Catal. A 160 (1997) 55.
[23] O.V. Buyevskaya, M. Baerns, Catalysis 16 (2002) 155.
[24] J. Hu, T. Xing, Q. Jia, H. Hao, D. Yang, Y. Guo, X. Hu, Appl. Catal. A 306 (2006) 29.
[25] Y. Ji, W. Li, H. Xu, Y. Chen, Appl. Catal. A 213 (2001) 25.
[26] Q. Jing, H. Lou, J. Fei, Z. Hou, X. Zheng, Int. J. Hydr. Energy 29 (2004) 1245.
[27] V.A. Tsipouriari, Z. Zhang, X.E. Verykios, J. Catal. 179 (1998) 283.
[28] Q.G. Yan, W.Z. Weng, H.L. Wan, H. Toghiani, R.K. Toghiani, C.U. Pittman, Appl. Catal. A 239 (2003) 43.
[29] J.H. Lunsford, Oxidative Coupling of Methane, Wiley-VCH, Weinheim, 1997, p. 1843.
[30] R. Jin, Y. Chen, W. Li, W. Cui, Y. Ji, C. Yu, Y. Jiang, Appl. Catal. A 201 (2000) 71.
[31] J.Z. Luo, Z.L. Yu, C.F. Ng, C.T. Au, J. Catal. 194 (2000) 198.
[32] V.C.H. Kroll, H.M. Swaan, S. Lacombe, C. Mirodatos, J. Catal. 164 (1996) 387.
[33] Y. Cui, H. Zhang, H. Xu, W. Li, Appl. Catal. A 318 (2007) 79–88.
[34] H.H. Wang, C. Tablet, T. Schiestel, J. Caro, Catal. Today 118 (2006) 98.
[35] C. Wagner, Progr. Solid State Chem. 10 (1975) 3.